ACS Sustainable Chemistry & Engineering

Research Article

Cite This: ACS Sustainable Chem. Eng. 2020, 8, 1043−1049

pubs.acs.org/journal/ascecg

High-Performance Lithium Ion Batteries Combining Submicron Silicon and Thiophene−Terephthalic Acid-Conjugated Polymer Binders

Kuo-Lung Wang,[†] Kuan-Ting Chen,[†] Yuan-Hsing Yi, Yi-Hao Hung, Hsing-Yu Tuan,* and Masaki Horie*

Department of Chemical Engineering, National Tsing Hua University, 101, Sec. 2, Kuang-Fu Road, Hsinchu 30013, Taiwan

Supporting Information

ABSTRACT: We developed high-performance lithium ion batteries (LIBs) based on submicron-sized recycled silicon and conjugated polymer binders. The polymer binders were synthesized by palladium-catalyzed direct arylation of 3-(2-ethylhexhyl)thiophene or 3,3′-di(2-ethylhexyl)bithiophene and dimethyl-2,5-dibromoterephthalate, followed by saponification. The LIBs were fabricated using composites of submicron-sized silicon and the polymer binders without conductive carbon additives. They exhibit a high capacity of up to 2700 mA h g^{-1} at a high rate of 1.0C, and 52% of this capacity is maintained even after 1000 cycles.

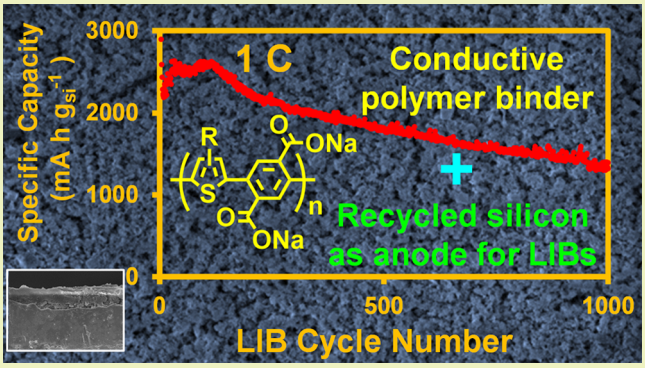

KEYWORDS: *lithium ion batteries, kerf loss silicon, submicron silicon, conjugated copolymers, direct arylation*

INTRODUCTION

Rechargeable energy storage devices such as lithium ion batteries (LIBs) have been developed intensively in response to increasing demand for their application in portable electronic devices and electric vehicles.[1−3] Current commercial LIBs consist of graphite as the anode material and achieve specific capacities up to 372 mA h g^{-1} with stability in the range of thousands of cycles.[4] However, their low capacity has limited their applications. To improve this capacity, various materials such as phosphorus, sulfur, and silicon have been used to substitute graphene.[5−9] In particular, silicon-based anode materials have high theoretical capacity, up to 4200 mA h g^{-1}, but three to four times volume expansion during cycling, leading to silicon cracking and eventually capacity fading.[10−12] To solve this issue, the components inside the battery configuration have been improved using porous silicon, nanosized silicon, and polymer binders.[13] In addition, the batteries' fabrication costs must be considered. Improving LIBs by involving nanosized silicon in the battery electrode increases their cost. Recently, the use of submicron-sized recycled silicon from the photovoltaic industry, the so-called kerf loss silicon, has been proposed as a solution to reduce the cost of the Si source for LiBs.[14−18] However, submicron-sized silicon is still prone to mechanical fracture upon cycling, which generally causes unstable LIB performances.[19]

Polymer binders are generally considered to maintain the connection between the active materials and the current collector.[20] Commercial polymer binders, such as poly(acrylic acid) (PAA), carboxymethyl cellulose (CMC), and poly(vinylidene difluoride) (PVDF), have been used for adhesion purposes.[21,22] However, due to their electric insulating properties, these polymers require conductive additives such as carbon materials, which reduce the overall volumetric capacity.[23] Utilization of conductive polymer binders allows simplification of the battery configuration because they can both facilitate charge transport and improve elastic properties.[2,24,25] Liu and Yang et al. reported the combination of a conductive polyfluorene derivative and nanosized silicon for developing an anode electrode in LIBs, which gave a high capacity of 2000 mA h g^{-1} over 650 cycles at 0.1C.[26] After their report, various conductive binders such as a polymer matrix with PEDOT:PSS and polyaniline derivative for silicon anode LIBs have been reported.[27−32] Recently, water-soluble polyfluorenes with the −COONa group were reported for use in silicon-based LIBs, giving a stable capacity of 1000 mA h g^{-1} for 1000 cycles at 1.0C.[33,34]

The synthesis of typical conjugated copolymers has been achieved by cross-coupling polycondensations, such as Suzuki and Stille couplings, which require functionalization of monomers with boronic acid or toxic organostannyls.[35−38] To simplify these synthesis procedures, the use of direct arylation polymerization[39−41] is a possible solution because this method can directly provide conjugated polymers without

Received: September 30, 2019
Revised: December 7, 2019
Published: December 25, 2019

DOI: 10.1021/acssuschemeng.9b05800
ACS Sustainable Chem. Eng. 2020, 8, 1043−1049

complicated functional groups, potentially leading to environmentally friendly and scalable polymers for electronic applications at a low cost.[42−44] Recently, we reported synthesizing alternating copolymers comprising cyclopentadithiophene and benzoic acid or terephthalic acid through direct arylation polymerization for use as polymer binders for silicon nanoparticles as anode electrode materials in LIBs.[45,46] To further improve the cycling life of silicon-based LIBs, it is essential to introduce hydrophilic side chains, such as the −COONa group, into conductive polymer binders, thus increasing the binding ability of polymers to silicon particles.[14−18,47,48]

Here, we report the synthesis of conjugated polymers comprising thiophene or bithiophene and terephthalic acid units by direct arylation polymerization followed by saponification. These polymers were used as conductive polymer binders with submicron-sized recycled silicon as the anode for LIBs. Figure 1 shows the transmission electron microscopic (TEM) image of the silicon−polymer composite and a summary of the advantages of this composite system. These highly covered silicon−polymer composites exhibit high capacity and stability at a high charge−discharge rate in LIBs.

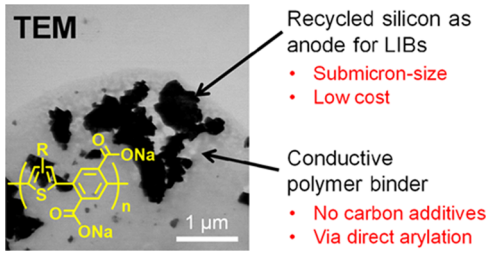

Figure 1. TEM image and advantages of the composite of poly[3-(2-ethylhexyl)thiophene-*alt*-2,5-terephthalic acid sodium salt] (PT1T) and submicron-sized recycled silicon.

RESULTS AND DISCUSSION

Scheme 1 and Table 1 (also Tables S1 and S2) summarize the synthesis of the polymers. 3-(2-Ethylhexhyl)thiophene or 3,3′-di(2-ethylhexyl)bithiophene and dimethyl-2,5-dibromoterephthalate were copolymerized by palladium-catalyzed direct arylation polymerization in the presence of $Pd(OAc)_2$, K_2CO_3, and neodecanoic acid to provide poly[3-(2-ethylhexyl)thiophene-*alt*-dimethyl-2,5-terephthalic acid] (PT1M) and poly[3,3′-bis(2-ethylhexyl)-2,2′-bithiophene-*alt*-dimethyl-2,5-terephthalic acid] (PT2M). The yield and the molecular weight of PT1M increased with the reaction temperature and time (Table S1); however, the insoluble residue also increased. As shown in Table 1, PT1M-1 (M_n = 3200, yield 23%) was prepared at 70 °C for 24 h, whereas PT2M-1 (M_n = 6500, yield 71%) was obtained at 70 °C for only 1 h. The lower yield of PT1M-1 than PT2M-1 is due to the lower reactivity of thiophene monomer than bithiophene monomer in direct arylation, and low molecular weight oligomers were washed off during precipitation and washing processes. It was reported that the bithiophene monomer was more reactive than the thiophene monomer in direct arylation polymerization due to the larger conjugated structure.[49]

Scheme 1. Synthesis of Polymers

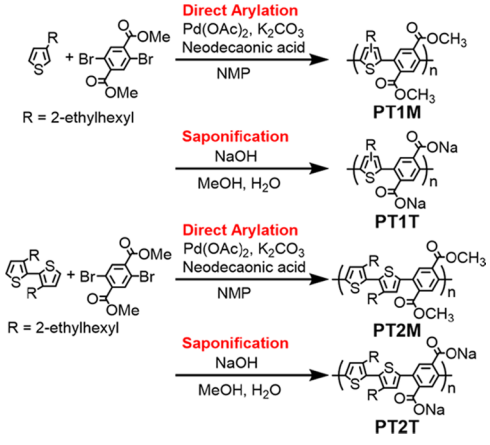

Table 1. Polymer Molecular Weight and Yield

polymer	temp. (°C)[a]	M_n[b]	M_w/M_n[b]	yield (%)
PT1M-1[c]	70	3200	1.33	23
PT1M-2	120	2600	1.18	38[f]
PT1T	60	NA[e]	NA[e]	87
PT2M-1[d]	70	6500	1.96	71
PT2M-2	120	NA[e]	NA[e]	8[f]
PT2T	60	NA[e]	NA[e]	77

[a]Reaction temperature for direct arylation or saponification. [b]Polymer molecular weight was estimated by gel permeation chromatography (GPC) using tetrahydrofuran (THF) eluent and polystyrene standards. [c]Reaction was carried out at 70 °C for 24 h. [d]Reaction was carried out at 70 °C for 1 h. [e]GPC measurement was inherently difficult due to the high polarity of the polymers. PT2M-2 was partially saponified by the high-temperature reaction in the presence of K_2CO_3. [f]Yield after Soxhlet extraction.

On the other hand, direct arylation polymerization potentially provides branched structures caused by the reaction on 4-position of thiophene. It was reported that carboxylic acid additives reduced such side reactions.[50] Therefore, we selected neodecanoic acid as an additive for the direct arylation polymerization. As shown in Figure S3, ^{1}H NMR of PT2M-1 showed singlet peaks at 7.80 and 6.93 ppm, which correspond to aromatic protons of dimethyltelephthalic acid and bithiophene, respectively. Other signals in the aromatic region were insignificant, suggesting that the branched structures were suppressed. In contrast, ^{1}H NMR of PT1M-1 (Figure S1) showed multiple peaks in the aromatic region, possibly due to the presence of regiorandom, branched, and partially saponified structures.

PT1M-1 and PT2M-1 were used for characterization and comparison of the reactivity between thiophene and bithiophene in direct arylation at 70 °C. On the other hand, PT1M-2 and PT2M-2, which were synthesized at a high temperature of 120 °C, were used for further treatment because they were obtained in a high reaction yield (99%), though the yield was decreased after Soxhlet extraction due to the production of the insoluble residue. After Soxhlet extraction, PT1M-2 and PT2M-2 were saponified by treatment with a NaOH aqueous solution to provide poly[3-(2-ethylhexyl)thiophene-*alt*-2,5-terephthalic acid sodium salt] (PT1T) and poly[3,3′-bis(2-ethylhexyl)-2,2′-bithiophene-*alt*-2,5-terephthalic acid sodium salt] (PT2T). The polymers were characterized by ^{1}H NMR (Figures S2 and S4) and FTIR spectroscopies (Figure S5). However, after saponification, GPC analysis of PT1T and PT2T was inherently difficult using methanol and water eluents, probably because of their strong

DOI: 10.1021/acssuschemeng.9b05800
ACS Sustainable Chem. Eng. 2020, 8, 1043−1049

hydrophilicity and polarity. The model reaction of the saponification was conducted for dimethyl-2,5-dibromotereph-thalate under similar reaction conditions with the polymers. The resulting product was analyzed by ^{1}H NMR spectroscopy, exhibiting 93% conversion from the −COOMe to −COONa group (Figures S6 and S7).

The electric conductivity (σ_{EC}) and ionic conductivity (σ_{IC}) of the polymers were estimated by the direct current 4-probe method and complex impedance analysis, respectively. These values are compared and summarized in Figure 2 and Table 2.

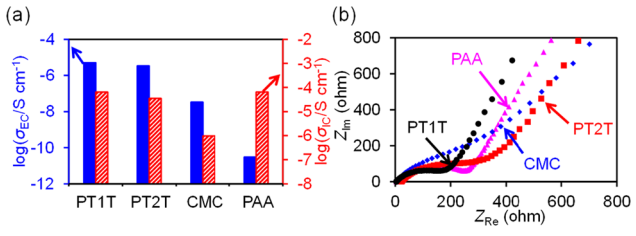

Figure 2. (a) Electric and ionic conductivities of PT1T, PT2T, CMC, and PAA. (b) Cole−Cole plot of the polymers.

Table 2. Electric and Ionic Conductivities of Polymers

materials	electric conductivity[a] (S cm^{-1})	ionic conductivity[b] (S cm^{-1})
PT1T	5.0×10^{-6}	6.5×10^{-5}
PT2T	3.4×10^{-6}	3.5×10^{-5}
CMC	3.3×10^{-8}	9.6×10^{-7}
PAA	3.0×10^{-11}	6.5×10^{-5}

[a]The electric conductivity was estimated by equation $\sigma_{EC} = (1/R) \times (d/A)$, where R is Ohmic resistance, d is the distance between electrodes, and A is the effective area for electron migration. [b]The ion conductivity was estimated by equation $\sigma_{IC} = (1/R) \times (d/S)$, where R is the charge transfer resistance, d is the thickness of the electrode, and S is the surface area of the electrode.

PT1T and PT2T showed $\sigma_{EC} = 5 \times 10^{-6}$ and 3×10^{-6} S cm^{-1}, respectively, which were 2−5 orders higher than those of conventional polymers, CMC (M_w = 90 000, $\sigma_{EC} = 3.3 \times 10^{-8}$ S cm^{-1}) and PAA (M_w = 3 000 000, $\sigma_{EC} = 3.0 \times 10^{-11}$ S cm^{-1}). Such high σ_{EC} values for PT1T and PT2T are probably due to their conjugated structures compared with nonconjugated polymers.[26,S1] PT1T and PT2T exhibited σ_{IC} in the order of 10^{-5} S cm^{-1}, which is 1 order higher than CMC, but in a similar order to PAA. Since σ_{IC} was measured in the presence of organic electrolytes, the polymer film should be swollen by the organic electrolytes for the ion migration to afford high σ_{IC}. PT1T and PT2T possess both hydrophobic 2-ethylhexyl and hydrophilic COONa groups; therefore, these polymers have an appropriate affinity with the organic electrolytes. CMC does not have such hydrophobic groups. PT1T showed slightly higher σ_{IC} than PT2T, probably because it contains a smaller number of hydrophobic 2-ethylhexyle side chains than PT2T. In addition, PT1T has a higher density of the −COONa group than PT2T, leading to higher ion migration. Consequently, PT1T is expected to be a good candidate for a conductive polymer binder in LIBs.

The battery performance was tested using half-coin cells fabricated using PT1T, PT2T, and CMC with submicron-sized silicon anode. Figure 3a shows the charging−discharging cycling performance of the LIBs for 100 cycles at the rate of 0.1C. Figure S9 shows their performance based on Coulomb efficiency. The LIB fabricated using PT1T exhibited the

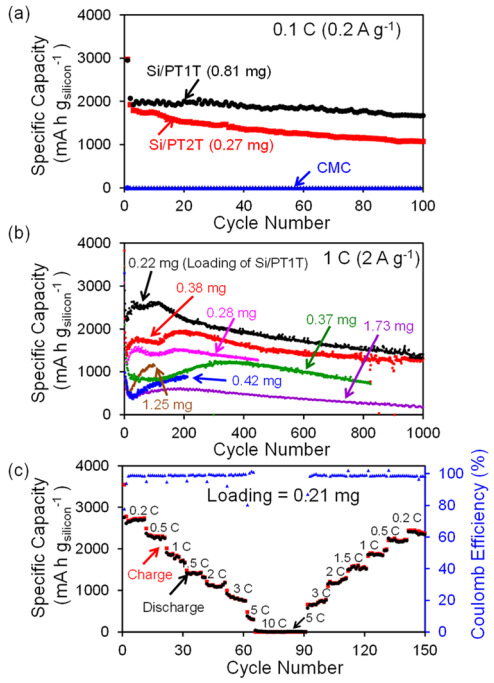

Figure 3. Cycling performance of LIBs composed of (a) PT1T, PT2T, and CMC at 0.1C (0.2 A g^{-1}) and (b) PT1T at 1.0C. (c) Stage cycling of LIB composed of PT1T from 0.2C to 10C. The electrode surface area: 1.13 cm^{-2}. 1.0C corresponds to 2000 mA h g^{-1} in this work.

highest specific capacity of 2077 mA h g^{-1} in the second cycle. After 100 cycles, the LIB still maintained a high specific capacity of 1677 mA h g^{-1}, which was 80% of the second cycle capacity. The LIB composed of PT2T exhibited slightly lower capacity compared to that of PT1T in the second cycle. However, this device retained 55% capacity after 100 cycles. LIB composed of CMC without carbon additives did not show any specific capacity.

As the LIB of PT1T exhibited the best specific capacity and stability, PT1T was selected for further optimization. Figures 3b and S11 show the cycling performance of LIBs at rates of 1.0C and 0.1C, respectively, with various loading weights of the composite material on the electrode. At 1.0C, the best device was obtained from the lowest loading (0.22 mg), exhibiting a specific capacity up to 2700 mA h g^{-1} with steady performance with 47% retention capacity after 1000 cycles. Meanwhile, the highest loading (1.73 mg) provided the lowest specific capacity and retained only 22% of the capacity after 1000 cycles. The best battery performance at 1.0C based on the Coulomb efficiency is shown in Figure S12. Due to the use of the fixed size of the coin cell, the mass loading of the active composite material directly affects the thickness of the electrode. The higher mass loading of the composite afforded thicker electrodes. It was reported that a thinner film showed better battery performance because less loading reduced total volume change during cycling, providing enhanced adhesion force on the current collector.[9] In contrast, a thicker film leads to the formation of cracks during cycling. Because the cracked parts were removed from the current collector, the transportation of electrons was inhibited, leading to declined battery performance.

Figure 3c shows the stage capacity of the LIB of PT1T with 0.21 mg of the composite loading at various rates. The LIB

DOI: 10.1021/acssuschemeng.9b05800
ACS Sustainable Chem. Eng. 2020, 8, 1043−1049

properly worked during charging and discharging at 0.2C, 0.5C, 1.0C, 1.5C, 2.0C, and 3.0C with ca. 100% efficiency. However, this LIB did not recover at 5.0C or 10.0C. After that, the capacity was recovered at 3.0C. At 0.2C, the retention capacity was 89% of the initial capacity.

Cyclic voltammetry (CV) measurements were performed at a scan rate of 0.1 mV s^{-1} in the potential window between 0 and 1.5 V versus Li/Li^+ (Figure S16). The PT1T-based silicon electrode showed two reduction peaks at 0.01 and 0.17 V, which reflects the lithiation process forming Li_XSi. The two oxidation peaks at 0.35 and 0.46 V are referred to as the delithiation process of lithium silicide. Also, electrochemical stability of the binder is required because it has to tolerate reductive reaction around 0−1.5 V.[31] The CV profiles of the electrode without Si exhibited lower current density than the electrode with Si, indicating that the binder has good electrochemical stability.

The surface morphologies of the electrodes were observed by scanning electron microscopy (SEM) and TEM (Figure 4).

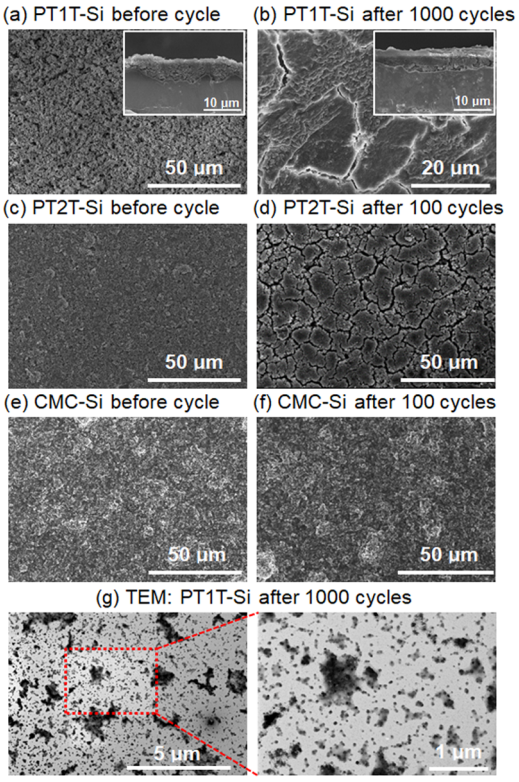

Figure 4. Electrode surface morphology of composite materials. SEM images of silicon−polymer composite composed of PT1T (a) before and (b) after cycling, PT2T (c) before and (d) after cycling, and CMC (e) before and (f) after cycling on the electrode. (g) TEM images of silicon−PT1T composite after 1000 cycles.

Figure 4a,c,e shows the SEM images of the PT1T, PT2T, and CMC composites with submicron-sized silicon on the electrode before cycling. The electrode surface comprising PT1T showed a smooth and uniform morphology, whereas PT2T showed tiny clusters, possibly due to the lower compatibility of PT2T with silicon than PT1T. In contrast, the composite of CMC and silicon exhibited large clusters and aggregations.

These surface morphologies were compared with those after cycling. As shown in Figure 4b, the composite of PT1T contained a smooth region after 1000 cycles at 1.0C, though it showed some cracks. The observed smooth region could be due to the formation of a stable solid electrolyte interphase (SEI) layer, where the charge transfer resistance was maintained for ion migration and contributed to maintaining the capacity steady during the long-term cycling.[10,11] As shown in the inset cross-sectional images in Figure 4a,b, the composite retained good adhesion ability on the electrode even after 1000 cycles. On the other hand, the PT2T composite had severe cracks after 100 cycles (Figure 4d). The composite of CMC still had numerous clusters and aggregations after 100 cycles (Figure 4e).

Figures 1 and 4g show TEM images of the PT1T composite with silicon before and after 1000 cycles, respectively. Before cycling, the random shapes with black color correspond to submicron-sized silicon particles, which were well covered by the PT1T polymer binder. Even after 1000 cycles, these silicon particles were still well covered, though the submicron-sized silicon particles were partially decomposed into nanosized fragments. These well-covered nanosized silicon particles are still active for charging/discharging and ion transportation through the polymer embedded electrode surface. Such well-covered Si is probably supported by strong adhesive property and high σ_{EC} and σ_{IC} of PT1T, causing efficient charge and ion transport during the 1000 cycles.

CONCLUSIONS

We developed high-performance LIBs with high specific capacity and stability at a high charging/discharging rate, using submicron-sized silicon and conjugated polymer binders. The battery performance was significantly improved compared to previously reported LIBs fabricated using nanosized Si with conjugated polymer binders such as poly-(cyclopentadithiophene-benzoic acid) and poly-(cyclopentadithiophene-terephthalic acid) (Table S3).[46] The LIBs' preparation procedure is simple, low cost, and environmentally friendly because it is based on using recycled silicon and direct arylated polymer binders. We expect such strategies to become very popular in the production of LIBs, organic electronics, and energy storage in the coming years.

EXPERIMENTAL SECTION

Synthesis of PT1M via Direct Arylation Polymerization. 3-(2-Ethylhexyl)thiophene (223 mg, 1.13 mmol), dimethyl-2,5-dibromoterephthalate (400 mg, 1.13 mmol), and potassium carbonate (465 mg, 3.36 mmol) were dissolved in anhydrous *N*-methyl-2-pyrrolidone (NMP) (1.1 mL) in a 25 mL Schlenk tube under nitrogen atmosphere. Palladium(II) acetate (36 mg, 0.14 equiv) and neodacanoic acid (90 mg) were subsequently added to the mixture, and the reaction mixture was stirred at room temperature for 10 min. This was then heated at 70 °C for 24 h. After cooling to room temperature, the reaction mixture was poured into cold methanol and washed with cold methanol five times. The residue was collected by centrifugation and dried in vacuum to obtain PT1M-1 (yield: 101 mg, 23%). ^{1}H NMR (500 MHz, $CDCl_3$): δ 8.01−6.87 (m, 2H, Ar-H), 3.82−3.744 (m, 3H, OCH_3), 2.71−2.35 (m, 2H, CH_2), 1.55−0.72 (m, 15H, 2-EH).

Similarly, 3-(2-ethylhexyl)thiophene (223 mg, 1.13 mmol), dimethyl-2,5-dibromoterephthalate (400 mg, 1.13 mmol), and potassium carbonate (465 mg, 3.36 mmol) were dissolved in anhydrous NMP (1.1 mL) in a 25 mL Schlenk tube under nitrogen atmosphere. Palladium(II) acetate (36 mg, 0.14 equiv) and neodacanoic acid (90 mg) were subsequently added to the mixture, and the reaction mixture was stirred at room temperature for 10 min. This was then heated at 120 °C for 24 h. After cooling to room

DOI: 10.1021/acssuschemeng.9b05800
ACS Sustainable Chem. Eng. 2020, 8, 1043−1049

temperature, the reaction mixture was poured into 200 mL of methylethyl ketone. The precipitated product was washed by Soxhlet extraction with methylethyl ketone (24 h), hexane (12 h), chloroform (12 h), and tetrahydrofuran (12 h) and extracted with ethanol (24 h). After being dried in vacuum, the residue was washed with 150 mL of methylethyl ketone, followed by washing with 5 mL of water. The residue was collected by centrifugation and dried in vacuum to obtain PT1M-2 (Yield: 165 mg, 38%). Other reaction conditions and results are summarized in Table S1.

Synthesis of PT1T via Saponification. PT1M-2 (165 mg, 0.42 mmol) was dissolved in methanol (85 mL) and 0.1 M sodium hydroxide aqueous solution (8.5 mL) in a 250 mL round-bottom flask. After stirring at 60 °C for 24 h under nitrogen atmosphere, the solution was dried at 50 °C in vacuum to obtain a green powder (yield: 150 mg, 88%). ^{1}H NMR (500 MHz, D_2O): δ 7.82−7.17 (m, 2H, Ar-H), 3.65−3.29 (m, remaining OCH_3), 2.44 (br, 2H, CH_2), 1.48 (s, 1H, CH), 1.13 (m, 8H, CH_2), 0.74 (m, 6H, CH_3).

Synthesis of PT2M via Direct Arylation Polymerization. A mixture of methyl 3,3′-di(2-ethylhexyl)bithiophene (222 mg, 0.56 mmol), dimethyl-2,5-dibromoterephthalate (200 mg, 0.56 mmol), and potassium carbonate (232 mg, 1.68 mmol) was dissolved in anhydrous NMP (0.56 mL) in a 10 mL Schlenk tube under nitrogen atmosphere. Palladium(II) acetate (18 mg, 0.14 equiv) and neodacanoic acid (45 mg) were subsequently added to the mixture, and the reaction mixture was stirred at room temperature for 10 min. This was then heated at 70 °C for 1 h. After cooling to room temperature, the reaction mixture was poured into cold methanol and washed with cold methanol five times. The residue was collected by centrifugation and dried in vacuum to obtain PT2M-1 (yield: 235 mg, 71%). ^{1}H NMR (500 MHz, $CDCl_3$): δ 7.80 (s, 1H, Ar-H), 6.93 (s, 1H, Ar-H), 3.78 (s, 3H, OCH_3), 2.47 (d, 2H, CH_2), 1.23 (m, 8H, CH_2), 0.82 (m, 6H, CH_3). GPC (eluent: THF, polystyrene standards): M_n = 6500, M_w/M_n = 1.96.

Similarly, a mixture of methyl 3,3′-di(2-ethylhexyl)bithiophene (444 mg, 1.13 mmol), dimethyl-2,5-dibromoterephthalate (400 mg, 1.13 mmol), and potassium carbonate (465 mg, 3.36 mmol) was dissolved in anhydrous NMP (1.1 mL) in a 25 mL Schlenk tube under nitrogen atmosphere. Palladium(II) acetate (36 mg, 0.14 equiv) and neodacanoic acid (90 mg) were subsequently added to the mixture, and the reaction mixture was stirred at room temperature for 10 min. This was then heated at 120 °C for 24 h. After cooling to room temperature, the reaction mixture was poured into 200 mL of methylethyl ketone. The precipitated product was washed by Soxhlet extraction with methylethyl ketone (24 h), hexane (12 h), chloroform (12 h), and tetrahydrofuran (12 h) and extracted with ethanol (24 h). The ethanol fraction was dried in vacuum, washed with 150 mL of methylethyl ketone, collected by centrifugation, and dried in vacuum to obtain PT2M-2 (yield: 55 mg, 8%). Other reaction conditions and results are summarized in Table S2.

Synthesis of PT2T via Saponification. PT2M-2 (50 mg, 0.086 mmol) was dissolved in 17 mL of methanol in a 100 mL round-bottom flask. After the addition of 0.1 M sodium hydroxide aqueous solution (1.7 mL), the reaction mixture was heated at 60 °C for 24 h under nitrogen atmosphere. The mixture was dried in vacuum to provide a green powder of PT2T (yield: 40 mg, 77%). ^{1}H NMR (500 MHz, D_2O): δ 7.7 (s, 2H, Ar-H), 7.3−7.2 (m, 2H, Ar-H), 2.5 (s, 4H, CH_2), 1.52-0.74 (m, 30H, 2-EH).

Fabrication of Half-Cell. The half-cells of lithium ion batteries were prepared in Galvanostatic cycling of coin cells system (CR2032). The establishment was prepared by the silicon−polymer composite as the working electrode and the lithium metal as the counter electrode. The polymer composites were simply prepared from the mixture of Kerf Loss silicon and conductive polymer at 1:1 weight ratio in ethanol solvent (20:20 mg in 450 μL ethanol). After 24 h of vigorous stirring, the homogeneous slurry part was blade cast on the Cu foil and then gradually dried at 100 °C under argon atmosphere for another day. After cutting by the pressed rolling machine, the coin-type half-cells were assembled in the sequence of polymer−silicon composite, microporous polyethylene, and lithium metal foil in an argon-filled glove box. The electrolyte was prepared by 1.0 M $LiPF_6$ in fluoroethylene carbonate and diethyl carbonate at a 1:1 volume ratio. The battery performance data were estimated using Maccor Series 4000 machine in the voltage range from 0.01−1.50 V (vs Li/Li^+).

■ ASSOCIATED CONTENT

Supporting Information

The Supporting Information is available free of charge at https://pubs.acs.org/doi/10.1021/acssuschemeng.9b05800.

Experimental details; synthesis of polymers; ATR-FTIR spectra of polymers; model reaction of saponification; material characterization data; battery performances (PDF)

■ AUTHOR INFORMATION

Corresponding Authors

*E-mail: hytuan@che.nthu.edu.tw (H.Y.T.).
*E-mail: mhorie@mx.nthu.edu.tw (M.H.).

ORCID

Hsing-Yu Tuan: 0000-0003-2819-2270
Masaki Horie: 0000-0002-7734-5694

Author Contributions

†K.-L.W. and K.-T.C. contributed equally to this work and share first authorship.

Funding

This work was financially supported by the Ministry of Science and Technology, Taiwan, and National Tsing Hua University (107Q2708E1).

Notes

The authors declare no competing financial interest.

■ REFERENCES

(1) Li, M.; Lu, J.; Chen, Z. W.; Amine, K. 30 Years of Lithium-Ion Batteries. *Adv. Mater.* **2018**, *30*, No. 1800561.

(2) Chen, H.; Ling, M.; Hencz, L.; Ling, H. Y.; Li, G. R.; Lin, Z.; Liu, G.; Zhang, S. Q. Exploring Chemical, Mechanical, and Electrical Functionalities of Binders for Advanced Energy-Storage Devices. *Chem. Rev.* **2018**, *118*, 8936−8982.

(3) Zubi, G.; Dufo-Lopez, R.; Carvalho, M.; Pasaoglu, G. The lithium-ion battery: State of the art and future perspectives. *Renewable Sustainable Energy Rev.* **2018**, *89*, 292−308.

(4) Blomgren, G. E. The Development and Future of Lithium Ion Batteries. *J. Electrochem. Soc.* **2017**, *164*, A5019−A5025.

(5) Nitta, N.; Lei, D. N.; Jung, H. R.; Gordon, D.; Zhao, E. B.; Gresham, G.; Cai, J.; Luzinov, I.; Yushin, G. Influence of Binders, Carbons, and Solvents on the Stability of Phosphorus Anodes for Li-ion Batteries. *ACS Appl. Mater. Interfaces* **2016**, *8*, 25991−26001.

(6) Chang, W. C.; Tseng, K. W.; Tuan, H. Y. Solution Synthesis of Iodine-Doped Red Phosphorus Nanoparticles for Lithium-Ion Battery Anodes. *Nano Lett.* **2017**, *17*, 1240−1247.

(7) Zhou, G. M.; Liu, K.; Fan, Y. C.; Yuan, M. Q.; Liu, B. F.; Liu, W.; Shi, F. F.; Liu, Y. Y.; Chen, W.; Lopez, J.; Zhuo, D.; Zhao, J.; Tsao, Y. C.; Huang, X. Y.; Zhang, Q. F.; Cui, Y. An Aqueous Inorganic Polymer Binder for High Performance Lithium-Sulfur Batteries with Flame-Retardant Properties. *ACS Cent. Sci.* **2018**, *4*, 260−267.

(8) Schmuch, R.; Wagner, R.; Horpel, G.; Placke, T.; Winter, M. Performance and cost of materials for lithium-based rechargeable automotive batteries. *Nat. Energy* **2018**, *3*, 267−278.

(9) Salah, M.; Murphy, P.; Hall, C.; Francis, C.; Kerr, R.; Fabretto, M. Pure silicon thin-film anodes for lithium-ion batteries: A review. *J. Power Sources* **2019**, *414*, 48−67.

(10) Jin, Y.; Zhu, B.; Lu, Z. D.; Liu, N.; Zhu, J. Challenges and Recent Progress in the Development of Si Anodes for Lithium-Ion Battery. *Adv. Energy Mater.* **2017**, *7*, No. 1700715.

DOI: 10.1021/acssuschemeng.9b05800
ACS Sustainable Chem. Eng. 2020, 8, 1043−1049

(11) Feng, K.; Li, M.; Liu, W. W.; Kashkooli, A. G.; Xiao, X. C.; Cai, M.; Chen, Z. W. Silicon-Based Anodes for Lithium-Ion Batteries: From Fundamentals to Practical Applications. *Small* **2018**, *14*, No. 1702737.
(12) Liu, Z. H.; Yu, Q.; Zhao, Y. L.; He, R. H.; Xu, M.; Feng, S. H.; Li, S. D.; Zhou, L.; Mai, L. Q. Silicon oxides: a promising family of anode materials for lithium-ion batteries. *Chem. Soc. Rev.* **2019**, *48*, 285−309.
(13) Gonzalez, A. F.; Yang, N. H.; Liu, R. S. Silicon Anode Design for Lithium-Ion Batteries: Progress and Perspectives. *J. Phys. Chem. C* **2017**, *121*, 27775−27787.
(14) Huang, T. Y.; Selvaraj, B.; Lin, H. Y.; Sheu, H. S.; Song, Y. F.; Wang, C. C.; Hwang, B. J.; Wut, N. L. Exploring an Interesting Si Source from Photovoltaic Industry Waste and Engineering It as a Li-Ion Battery High-Capacity Anode. *ACS Sustainable Chem. Eng.* **2016**, *4*, 5769−5775.
(15) Lin, C. T.; Huang, T. Y.; Huang, J. J.; Wu, N. L.; Leung, M. K. Multifunctional co-poly(amic acid): A new binder for Si-based micro-composite anode of lithium-ion battery. *J. Power Sources* **2016**, *330*, 246−252.
(16) Chou, C. Y.; Kuo, J. R.; Yen, S. C. Silicon-Based Composite Negative Electrode Prepared from Recycled Silicon-Slicing Slurries and Lignin/Lignocellulose for Li-Ion Cells. *ACS Sustainable Chem. Eng.* **2018**, *6*, 4759−4766.
(17) Hachichi, K.; Lami, A.; Zemmouri, H.; Cuellar, P.; Soni, R.; Ait-Amar, H.; Drouiche, N. Silicon Recovery from Kerf Slurry Waste: a Review of Current Status and Perspective. *Silicon* **2018**, *10*, 1579−1589.
(18) Wagner, N. P.; Tron, A.; Tolchard, J. R.; Noia, G.; Bellmann, M. P. Silicon anodes for lithium-ion batteries produced from recovered kerf powders. *J. Power Sources* **2019**, *414*, 486−494.
(19) Lee, B.; Liu, T. Y.; Kim, S. K.; Chang, H.; Eom, K.; Xie, L. X.; Chen, S.; Jang, H. D.; Lee, S. W. Submicron silicon encapsulated with graphene and carbon as a scalable anode for lithium-ion batteries. *Carbon* **2017**, *119*, 438−445.
(20) Chou, S. L.; Pan, Y. D.; Wang, J. Z.; Liu, H. K.; Dou, S. X. Small things make a big difference: binder effects on the performance of Li and Na batteries. *Phys. Chem. Chem. Phys.* **2014**, *16*, 20347−20359.
(21) Li, J.; Lewis, R. B.; Dahn, J. R. Sodium carboxymethyl cellulose - A potential binder for Si negative electrodes for Li-ion batteries. *Electrochem. Solid State Lett.* **2007**, *10*, A17−A20.
(22) Magasinski, A.; Zdyrko, B.; Kovalenko, I.; Hertzberg, B.; Burtovyy, R.; Huebner, C. F.; Fuller, T. F.; Luzinov, I.; Yushin, G. Toward Efficient Binders for Li-Ion Battery Si-Based Anodes: Polyacrylic Acid. *ACS Appl. Mater. Interfaces* **2010**, *2*, 3004−3010.
(23) Liu, T. F.; Tong, C. J.; Wang, B.; Liu, L. M.; Zhang, S. Q.; Lin, Z.; Wang, D. L.; Lu, J. Trifunctional Electrode Additive for High Active Material Content and Volumetric Lithium-Ion Electrode Densities. *Adv. Energy Mater.* **2019**, *9*, No. 1803390.
(24) Shi, Y.; Zhou, X. Y.; Yu, G. H. Material and Structural Design of Novel Binder Systems for High-Energy, High-Power Lithium-Ion Batteries. *Acc. Chem. Res.* **2017**, *50*, 2642−2652.
(25) Lopez, J.; Mackanic, D. G.; Cui, Y.; Bao, Z. N. Designing polymers for advanced battery chemistries. *Nat. Rev. Mater.* **2019**, *4*, 312−330.
(26) Liu, G.; Xun, S. D.; Vukmirovic, N.; Song, X. Y.; Olalde-Velasco, P.; Zheng, H. H.; Battaglia, V. S.; Wang, L. W.; Yang, W. L. Polymers with Tailored Electronic Structure for High Capacity Lithium Battery Electrodes. *Adv. Mater.* **2011**, *23*, 4679−4683.
(27) Shen, L. Y.; Shen, L.; Wang, Z. X.; Chen, L. Q. In Situ Thermally Cross-linked Polyacrylonitrile as Binder for High-Performance Silicon as Lithium Ion Battery Anode. *ChemSusChem* **2014**, *7*, 1951−1956.
(28) Kim, S. M.; Kim, M. H.; Choi, S. Y.; Lee, J. G.; Jang, J.; Lee, J. B.; Ryu, J. H.; Hwang, S. S.; Park, J. H.; Shin, K.; Kim, Y. G.; Oh, S. M. Poly(phenanthrenequinone) as a conductive binder for nano-sized silicon negative electrodes. *Energy Environ. Sci.* **2015**, *8*, 1538−1543.
(29) Higgins, T. M.; Park, S. H.; King, P. J.; Zhang, C.; McEvoy, N.; Berner, N. C.; Daly, D.; Shmeliov, A.; Khan, U.; Duesberg, G.; Nicolosi, V.; Coleman, J. N. A Commercial Conducting Polymer as Both Binder and Conductive Additive for Silicon Nanoparticle-Based Lithium-Ion Battery Negative Electrodes. *ACS Nano* **2016**, *10*, 3702−3713.
(30) Zeng, W. W.; Wang, L.; Peng, X.; Liu, T. F.; Jiang, Y. Y.; Qin, F.; Hu, L.; Chu, P. K.; Huo, K. F.; Zhou, Y. H. Enhanced Ion Conductivity in Conducting Polymer Binder for High-Performance Silicon Anodes in Advanced Lithium-Ion Batteries. *Adv. Energy Mater.* **2018**, *8*, No. 1702314.
(31) Wang, L.; Liu, T. F.; Peng, X.; Zeng, W. W.; Jin, Z. Z.; Tian, W. F.; Gao, B.; Zhou, Y. H.; Chu, P. K.; Huo, K. F. Highly Stretchable Conductive Glue for High-Performance Silicon Anodes in Advanced Lithium-Ion Batteries. *Adv. Funct. Mater.* **2018**, *28*, No. 1704858.
(32) Lee, K.; Kim, T. H. Poly(aniline-co-anthranilic acid) as an electrically conductive and mechanically stable binder for high-performance silicon anodes. *Electrochim. Acta* **2018**, *283*, 260−268.
(33) Liu, D.; Zhao, Y.; Tan, R.; Tian, L. L.; Liu, Y. D.; Chen, H. B.; Pan, F. Novel conductive binder for high-performance silicon anodes in lithium ion batteries. *Nano Energy* **2017**, *36*, 206−212.
(34) Zhao, Y.; Yang, L. Y.; Zuo, Y. X.; Song, Z. B.; Liu, F.; Li, K.; Pan, F. Conductive Binder for Si Anode with Boosted Charge Transfer Capability via n-Type Doping. *ACS Appl. Mater. Interfaces* **2018**, *10*, 27795−27800.
(35) Lee, J.; Kalin, A. J.; Yuan, T. Y.; Al-Hashimi, M.; Fang, L. Fully conjugated ladder polymers. *Chem. Sci.* **2017**, *8*, 2503−2521.
(36) Hazari, N.; Melvin, P. R.; Beromi, M. M. Well-defined nickel and palladium precatalysts for cross-coupling. *Nat. Rev. Chem.* **2017**, *1*, No. 0025.
(37) Sun, C. K.; Pan, F.; Bin, H. J.; Zhang, J. Q.; Xue, L. W.; Qiu, B. B.; Wei, Z. X.; Zhang, Z. G.; Li, Y. F. A low cost and high performance polymer donor material for polymer solar cells. *Nat. Commun.* **2018**, *9*, No. 743.
(38) Zhou, D.; Tan, X. Y.; Wu, H. M.; Tian, L. H.; Li, M. Synthesis of C-C Bonded Two-Dimensional Conjugated Covalent Organic Framework Films by Suzuki Polymerization on a Liquid-Liquid Interface. *Angew. Chem., Int. Ed.* **2019**, *58*, 1376−1381.
(39) Biffis, A.; Centomo, P.; Del Zotto, A.; Zeccal, M. Pd Metal Catalysts for Cross-Couplings and Related Reactions in the 21st Century: A Critical Review. *Chem. Rev.* **2018**, *118*, 2249−2295.
(40) Gobalasingham, N. S.; Thompson, B. C. Direct arylation polymerization: A guide to optimal conditions for effective conjugated polymers. *Prog. Polym. Sci.* **2018**, *83*, 135−201.
(41) Blaskovits, J. T.; Leclerc, M. C-H Activation as a Shortcut to Conjugated Polymer Synthesis. *Macromol. Rapid Commun.* **2019**, *40*, No. 1800512.
(42) Guo, K.; Bai, J. H.; Jiang, Y.; Wang, Z. L.; Sui, Y.; Deng, Y. F.; Han, Y.; Tian, H. K.; Geng, Y. H. Diketopyrrolopyrrole-Based Conjugated Polymers Synthesized via Direct Arylation Polycondensation for High Mobility Pure n-Channel Organic Field-Effect Transistors. *Adv. Funct. Mater.* **2018**, *28*, No. 1801097.
(43) Ichige, A.; Saito, H.; Kuwabara, J.; Yasuda, T.; Choi, J. C.; Kanbara, T. Facile Synthesis of Thienopyrroledione-Based pi-Conjugated Polymers via Direct Arylation Polycondensation under Aerobic Conditions. *Macromolecules* **2018**, *51*, 6782−6788.
(44) Aldrich, T. J.; Dudnik, A. S.; Eastham, N. D.; Manley, E. F.; Chen, L. X.; Chang, R. P. H.; Melkonyan, F. S.; Facchetti, A.; Marks, T. J. Suppressing Defect Formation Pathways in the Direct C-H Arylation Polymerization of Photovoltaic Copolymers. *Macromolecules* **2018**, *51*, 9140−9155.
(45) Wang, K. L.; Kuo, T. H.; Yao, C. F.; Chang, S. W.; Yang, Y. S.; Huang, H. K.; Tsai, C. J.; Horie, M. Cyclopentadithiophene-benzoic acid copolymers as conductive binders for silicon nanoparticles in anode electrodes of lithium ion batteries. *Chem. Commun.* **2017**, *53*, 1856−1859.
(46) Yao, C. F.; Wang, K. L.; Huang, H. K.; Lin, Y. J.; Lee, Y. Y.; Yu, C. W.; Tsai, C. J.; Horie, M. Cyclopentadithiophene-Terephthalic Acid Copolymers: Synthesis via Direct Arylation and Saponification

DOI: 10.1021/acssuschemeng.9b05800
ACS Sustainable Chem. Eng. 2020, 8, 1043−1049

and Applications in Si-Based Lithium-Ion Batteries. *Macromolecules* **2017**, *50*, 6924−6934.
(47) Das, S.; Chatterjee, D. P.; Ghosh, R.; Nandi, A. K. Water soluble polythiophenes: preparation and applications. *RSC Adv.* **2015**, *5*, 20160−20177.
(48) Hu, B. L.; Wang, C. Y.; Zhang, J.; Qian, K.; Chen, W. Q.; Lee, P. S.; Zhang, Q. C. Water-soluble conjugated polymers as active elements for organic nonvolatile memories. *RSC Adv.* **2015**, *5*, 30542−30548.
(49) Fujinami, Y.; Kuwabara, J.; Lu, W.; Hayashi, H.; Kanbara, T. Synthesis of Thiophene- and Bithiophene-Based Alternating Copolymers via Pd-Catalyzed Direct C−H Arylation. *ACS Macro Lett.* **2012**, *1*, 67−70.
(50) Rudenko, A. E.; Thompson, B. C. Influence of the Carboxylic Acid Additive Structure on the Properties of Poly(3-hexylthiophene) Prepared via Direct Arylation Polymerization (DArP). *Macromolecules* **2015**, *48*, 569−575.
(51) Wu, M.; Xiao, X.; Vukmirovic, N.; Xun, S.; Das, P. K.; Song, X.; Olalde-Velasco, P.; Wang, D.; Weber, A. Z.; Wang, L. W.; Battaglia, V. S.; Yang, W.; Liu, G. Toward an ideal polymer binder design for high-capacity battery anodes. *J. Am. Chem. Soc.* **2013**, *135*, 12048−12056.

DOI: 10.1021/acssuschemeng.9b05800
ACS Sustainable Chem. Eng. 2020, 8, 1043−1049